Soft Matter

PAPER

Cite this: *Soft Matter*, 2014, **10**, 7647

Interfacial stability and shape change of anisotropic endoskeleton droplets

Marco Caggioni,[a] Alexandra V. Bayles,[b] Jessica Lenis,[a] Eric M. Furst[b] and Patrick T. Spicer*[c]

Received 8th July 2014
Accepted 4th August 2014

DOI: 10.1039/c4sm01482k

www.rsc.org/softmatter

The delivery of suspended active ingredients to a surface is a central function of numerous commercial cosmetic, drug, and agricultural formulations. Many products use liquid droplets as a delivery vehicle but, because interfacial tension keeps droplets spherical, these materials cannot exploit the benefits of anisotropic shape and shape change offered by solid colloids. In this work, individual droplet manipulation is used to produce viscoelastic droplets that can stably retain non-spherical shapes by balancing the Laplace pressure of the liquid–liquid interface with the elasticity of an internal crystalline network. A stability criterion is developed for idealized spherocylindrical droplets and shown to agree with experimental data for varying droplet size and rheology. Shape change can be induced in the anisotropic droplets by upsetting the balance of droplet interfacial tension and internal rheology. Using dilution to increase the interfacial tension shows that external stimuli can trigger collapse and shape change in these droplets. The droplets wrap around substrates during collapse, improving contact and adhesion. The model is used to develop design criteria for production of droplets with tunable response.

1 Introduction

Complex-shaped solid colloids have been created by droplet templating and assembly,[1,2] stop-flow lithography,[3] and micron-scale molding[4] and are known to be useful for active ingredient delivery because of preferential uptake[5] and flow behavior.[6] Shaped colloids are also promising building blocks for self-assembly into complex ordered structures[7] with applications in optics[8] and biomimicry.[9] Colloids that can change their shape can enhance self-assembly,[10] rheology control,[11] and drug delivery[12,13] and their shape can be altered by temperature changes,[14] volume change of composite particles,[15] or buckling,[16] but again only for solid colloids. When liquids are used in colloidal shape-change processes it is typically as a minor component of a solid particle, usually to drive movement by liquid–liquid[17] or liquid–air[18] interfacial tension.

Despite the many innovations in controlled synthesis of shaped, and shape-changing, solid colloids,[7] numerous commercial products still deliver active ingredients from emulsion droplets because they can be easier to prepare, enable dissolution of multiple compounds, and wet and adhere to substrates like hair,[19] skin, and internal tissue.[20] There is a significant opportunity to apply the advantages of controlled shape, and shape change, to droplet systems but the ability to control shape in droplets has only recently become possible in synthetic systems. Shape change is, however, quite common in biological cells[21] that possess many fluid properties and can change shape in response to interfacial/environmental triggers by altering their internal mechanical properties.[22]

Crudely analogous to cellular shapes, non-spherical droplet shapes can be stably formed by arrested coalescence in emulsions when interfacial[23] or internal[24] elasticity balances droplet interfacial stress,[8,25] halting coalescence at an intermediate state. Arrest by an internal elastic skeleton[24,26,27] is quite general and can be used to assemble structured droplets into non-spherical shapes, all while preserving a liquid surface with a curvature shaped by capillary forces.[24] Taking cellular architecture as an inspiration, anisotropic droplets with a viscoelastic internal crystalline microstructure are created here *via* molding. A physical model of their stability is developed and tested by microscopic observations of shape stability while varying droplet rheology and size. The endoskeleton droplets are shown to change their shape in response to dilution-induced increases in interfacial tension, also in agreement with the physical model. Droplet shape change is shown to enhance adhesion and wetting of substrates, offering a route to improve delivery of droplet materials to a number of surfaces of interest and supplementing the properties of solid particles with a droplet's ability to wet a surface and deliver solutes *via* diffusion. Although a single rod shape is studied here, the molding of droplets with other shapes is also possible and the theoretical stability criterion may be extended to describe other shapes as well.

[a]*Complex Fluid Microstructures, Corporate Engineering, Procter and Gamble Co, 8256 Union Center Blvd, West Chester, Ohio, USA*

[b]*Department of Chemical and Biomolecular Engineering and Center for Molecular and Engineering Thermodynamics, University of Delaware, Newark, DE, USA*

[c]*School of Chemical Engineering, UNSW Australia, Sydney, Australia. E-mail: p.spicer@unsw.edu.au*

2 Experimental details

A mixture of hexadecane (99%, Sigma Aldrich) and petrolatum (Unilever) yields droplets that can be molded into specific shapes by melting and recrystallizing a constrained droplet. Molding and manipulation of shaped droplets can be induced and observed on a microscope stage fitted for micromanipulation. Tapered borosilicate glass capillaries (1 mm OD and 0.5 mm ID, Sutter Instruments) are made with a Micropipette Puller (Model P-97; Sutter Instruments). The tip of a pulled capillary is flattened with a Microforge (Model MF-830; Narishige Intl. USA). The other end of the capillary is connected to a water reservoir (10 mL open syringe) by rubber tubing. Adjusting water reservoir height adjusts the hydrostatic pressure at the flat end of the capillary, enabling grasping and manipulation of droplets. Water can also be pumped into the system *via* pressure applied to the syringe. The capillary is mounted on a 3-axis coarse manipulator (Narishige Intl USA) attached to a microscope stage (Zeiss Axioplan-2). A one mL diluted drop of emulsion is placed on a glass slide and the tip of the mounted capillary aligned with one of the droplets using the micromanipulator. The droplet is drawn toward the capillary by applying negative hydrostatic pressure. Suction is adjusted to just hold the droplet stationary at the capillary tip. Individual droplet study is made easier by a small yield stress, created with 0.5% microfibrous cellulose (CP-Kelco) in an aqueous 10 mM solution of sodium dodecyl sulfate (Fluka). Melting of the droplet microstructure is performed on a computer-controlled heated microscope stage (Linkham THMS 600). The bulk yield stress of the droplet mixture is determined by measuring its elastic modulus as a function of strain on a TA Instruments G2 rheometer. Measurements are made at a frequency of 1 Hz as the elastic modulus exhibits no frequency dependence between 0.01 and 1 Hz. The critical strain is determined to be the point at which the elastic modulus drops rapidly and the yield stress is calculated as the product of the plateau modulus and the critical strain. Droplet interfacial tension is measured using a Kruss DSA100 pendant drop tensiometer.

3 Results and discussion

Droplets contain a mixture of hexadecane and petrolatum, and the proportion of the two determines the droplet elastic modulus and yield stress. Fig. 1 shows the variation of bulk yield stress for hexadecane containing a range of petrolatum levels. Droplet yield stress is a critical variable controlling stability of shaped droplets and the petrolatum level is seen in Fig. 1 to enable variation over at least two orders of relevant magnitude. The scaling of the yield stress follows a power-law with concentration in agreement with past work on anistotopic colloid gels.[28,29] A typical experiment consists of producing an emulsion by hand mixing hexadecane and petrolatum with aqueous 10 mM sodium dodecyl sulfate. The molding of a rod-shaped droplet shape is performed by pulling the entire droplet into a microcapillary, heating the sample above the wax melting point of ~65 °C for 15 minutes, cooling for another 15 minutes, then ejecting the molded droplet. Fig. 2a shows a sequence of

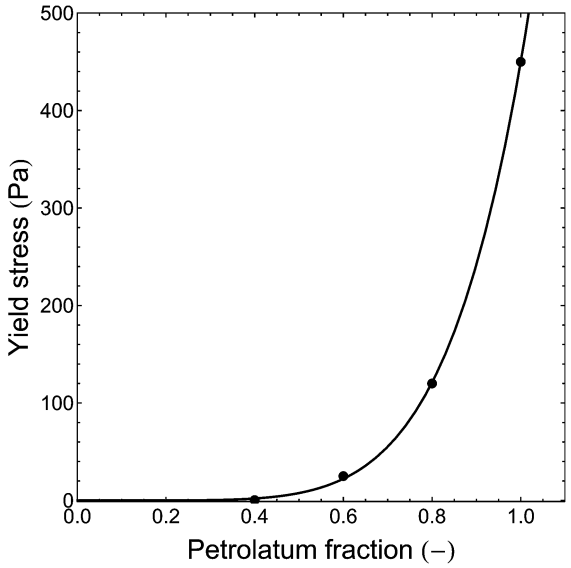

Fig. 1 The yield stress of hexadecane droplets increases steeply with added petrolatum solids, following a power law with exponent 5.9. The solid line is a power law fit to the data.

such steps and the ejection of a rod-shaped droplet that moves as a rigid body but still retains its liquid surface character because the oil completely wets the internal porous crystalline network. The yield stress of this droplet is 450 Pa as it contains 100% petrolatum and is sufficient to resist the interfacial pressure of the surrounding aqueous solution. Fig. 2b shows an unsuccessful attempt at molding, where a rod collapses on itself in stages as it is ejected. Here the droplet contains only 60% petrolatum, with a markedly lower yield stress of 25 Pa, to oppose the constant interfacial pressure exerted by the continuous phase fluid to shape the droplet into a sphere. When fully outside of the capillary, the rod has collapsed to a roughly

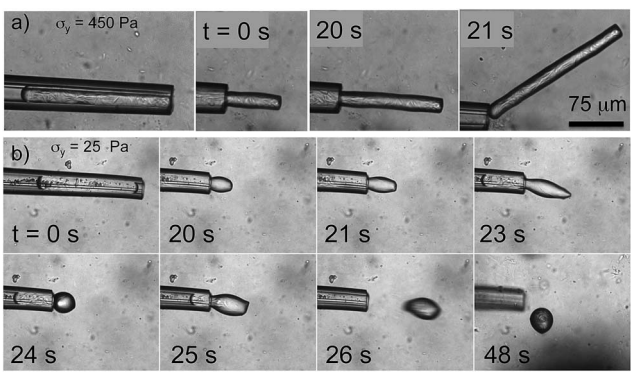

Fig. 2 (a) Rod-shaped endoskeleton droplets are produced by suctioning a spherical droplet into a micro capillary, heating to melt the skeleton, then recrystallizing the skeleton while molding by confinement. Once solid, the rod is ejected from the capillary by hydrostatic pressure and stably retains the capillary shape in the fluid environment. (b) Failure of a droplet as a result of insufficient solid content prior to ejection. Once removed from the mold, the force of the external fluid interfacial pressure causes the rod to buckle and yield as soon as it exits the capillary.

spherical droplet again with little indication of the internal solids present. Comparison of the two droplets in their spherical and rod-shaped states indicates the increased collision profile of the latter and its potential modification of flow, and other droplet properties, when its non-spherical shape is stable. The molding of a specific droplet shape, even a simple rod, demonstrates the ability of endoskeleton droplets to combine the utility of shaped solid colloids with the flexibility of liquid droplets. Such droplets allow creation of a desired droplet size and shape for use in targeted applications, if the interfacial and rheological properties needed for stability can be determined.

Fig. 3 shows a schematic and force balance for an idealized model of the rod in Fig. 2a, a spherocylinder, where the hemispherical end caps reflect the dominance of the droplet interface's liquid character. The force on such a structure can be modeled by extending a previous theoretical model, of arrested coalescence in spherical structured droplets,[24] to account for nonlinear as opposed to linear elastic deformation. For a droplet with internal microstructure, stress is applied by the droplet interfacial tension on the internal elastic structure, deforming it and producing an elastic reaction. For sufficiently strong elastic structures, the interfacial pressure is offset and stable anisotropic shapes are obtained. By generalizing this model we expect that elastic endoskeletons, inside emulsion droplets distorted into anisotropic shapes, always experience a compressive stress not offset by the incompressible nature of the liquid phase. The compressive stress, σ_i, due to the interfacial tension, γ, should be of the order of the Laplace pressure applied by the two hemispherical caps with radius R_{cap} on the cylindrical section in Fig. 3:

$$\sigma_i = \frac{2\gamma}{R_{cap}} \quad (1)$$

When the pressure exerted by the interfacial tension, γ, cannot overcome the yield stress, σ_y, of the endoskeleton, $\sigma_i < \sigma_y$, the droplet can maintain its shape by keeping the liquid interface deformed. In contrast, when this condition is not fulfilled, the structure yields and the particle shape relaxes toward a less anisotropic shape. The critical minimum cap radius R_{cap}^{min} is then:

$$R_{cap}^{min} = \frac{2\gamma}{\sigma_y} \quad (2)$$

so that with a constant γ, the rod's yield stress and maximum surface curvature, $1/R_{cap}^{min}$, rather than aspect ratio, determine rod stability. An interesting prediction of this model is that any length rod-shaped droplet is stable provided interfacial tension and rod radius are appropriate for a given endoskeleton's mechanical properties. This prediction is consistent with our observations of stable rods at aspect ratios as high as 30, as collapse only occurs when the yield stress is insufficient for a given rod end cap radius and the resulting interfacial pressure.

Plotting eqn (1) in Fig. 4 produces a design guide for rod-shaped droplets that maps regions of stability, where yield stress offsets interfacial pressures, and instability where the converse is true. Data for individual droplets, produced using the method in Fig. 2, are plotted based on microscopic observations of stability for at least 15 minutes. Using the measured interfacial tension of $\gamma = 1.5$ mN m^{-1}, the data match well with no fitting needed. Seven different stable rods, like the one in Fig. 2a but with different dimensions, are predicted to be stable as they are above and to the right of the stability boundary, where yield stress is high and curvature is low. At lower radii and yield stress, rods collapse immediately following production as in Fig. 2b. The smallest stable rods that we have consistently produced have an $R_{cap}^{min} = 10$ μm and a yield stress of $\sigma_y = 450$ Pa, above the stability boundary in Fig. 4. Intermediate between the above two cases are droplets produced on, or very near, the stability boundary. Such droplets are stable but are relatively close to the conditions of instability.

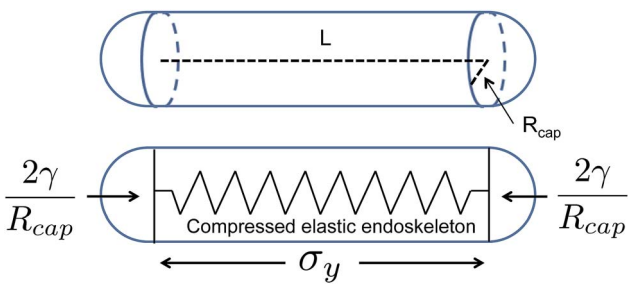

Fig. 3 Droplet stability is modeled using an ideal spherocylinder geometry that experiences a compressive stress from the Laplace pressure at either end and is opposed by the elasticity of the internal network.

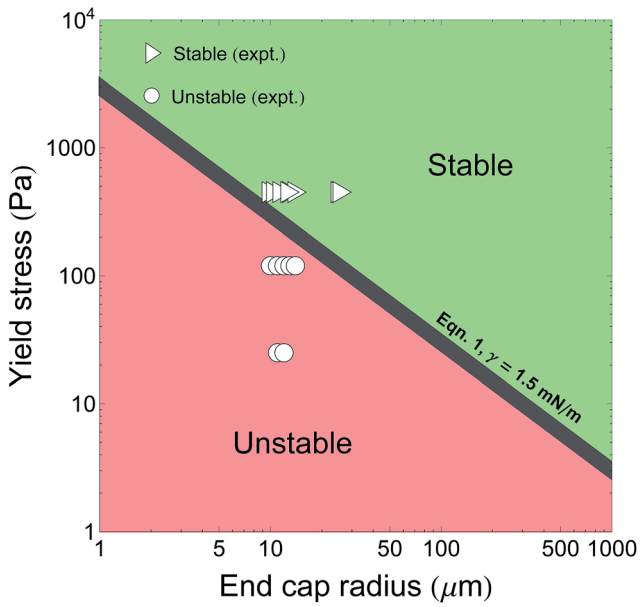

Fig. 4 Eqn (1) maps the boundary between predicted stability and instability of structured droplets. Plotted points indicate good agreement of experimental observations with the theory's predictions for a number of droplets with varying dimensions and yield stress values.

The model, along with the results of Fig. 2b, predicts that collapse of an endoskeleton droplet can occur due to insufficient mechanical strength, but it also points to a way to harness such behavior. If a rod is made with a yield stress stable against the lower interfacial tension of a concentrated surfactant product, like a commercial emulsion formulation, the rod can also be designed to collapse with a specific trigger, for example an increase in droplet interfacial tension caused during dilution or rinsing of a formulation during use. Fig. 4 can thus be used to design a rod of a certain dimension that is stable but close to instability, by adjusting its yield stress (Fig. 1) to be near the stability boundary in Fig. 4. Then an increase in interfacial tension, by dilution or rinsing, will shift the stability boundary up and suddenly place the droplet in the instability region. The micromanipulation approach allows us to test single droplet response to such external stimuli. Fig. 5 shows an endoskeleton rod held while a second capillary sprays it with deionized water. The response to the washing is immediate: the rod folds at each end due to a structural failure near the contact with the first capillary. The interfacial tension is clearly acting at all times on the endoskeleton droplet surface and any upset in the balance of forces with the skeleton will cause a shift to a new shape and state. As in Fig. 2b, the final state of the droplet is several times more compact than the starting rod shape, reducing from an aspect ratio of 7.7 to 1 during the collapse. In this case, however, the collapse of a formerly stable shape is only triggered by a change of external conditions.

The transition from stability to instability triggered by dilution in Fig. 5 can be studied in the context of a change in position of the stability boundary described by eqn (1). Fig. 6a plots the initial state of the droplet and its aqueous environment in Fig. 5, showing the droplet occupies the stability boundary area. Upon dilution, the stability boundary shifts upward, as seen in Fig. 6b, because of the increased interfacial tension. Consistent with the observations in Fig. 5, the droplet is now too weak to withstand the compression forces acting along its center axis and its collapse into a sphere is rapid. A similar approach can be used to design droplets for a specific application by adjusting the droplet strength *via* its yield stress to withstand its normal interfacial environment but fail during use or aging to aid performance.

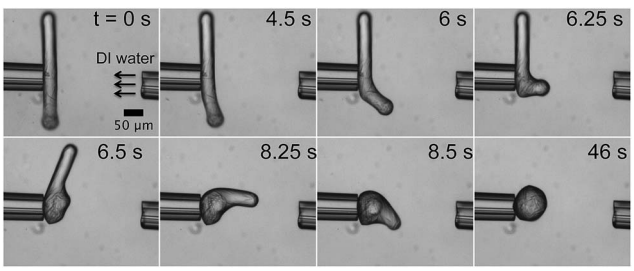

Fig. 5 Failure of an endoskeleton rod can be induced by increasing the local interfacial tension *via* washing away the locally adsorbed surfactant. Here a rod that is stable against the surfactant-lowered interfacial tension fails immediately upon washing with a stream of deionized water.

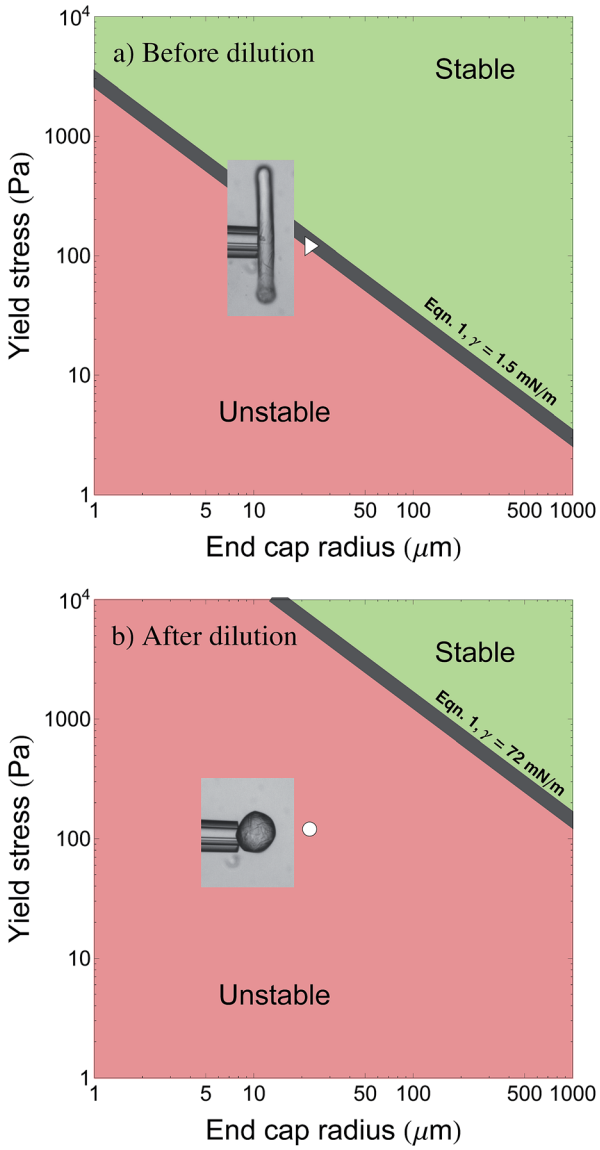

Fig. 6 Two states of the stability map for the rod in Fig. 5 showing (a) before and (b) after dilution with deionized water. The inset image shows the state of the droplet and the plotted data point indicates the relative position and stability of the droplet in each state. Initially the droplet is on the stability boundary and retains its anisotropic shape. Dilution raises the local interfacial tension, shifting the stability boundary upwards, yielding the droplet microstructure, and returning it to a spherical shape.

Stable, shaped droplets combine the utility of a non-spherical shape with the opportunity to change that shape when desired. Because the shape-change is driven by instantaneous interfacial pressure gradients, a directional component can be added by biasing the collapse toward a point of contact with another surface, like a hair, clothing fiber, or plant stalk, for example. Fig. 7 shows a rod in contact with a Teflon fiber over less than half of its length. When deionized water is released in the nearby fluid *via* microcapillary, the rod collapses and wraps itself around the fiber over its entire length for an increase in contact area of more than 100%. The last image's enhanced

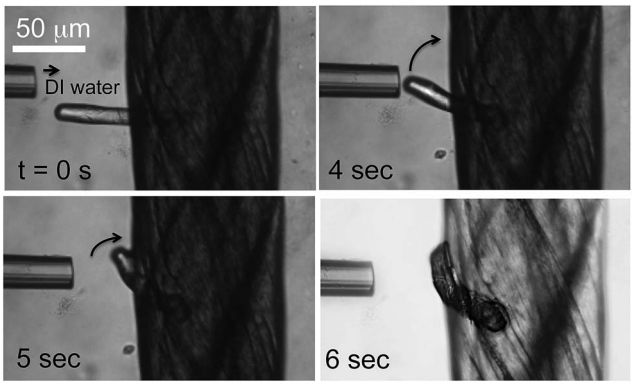

Fig. 7 Collapse of a rod can be harnessed to improve adhesion and retention on targeted surfaces, like the Teflon fiber shown here. A rod is first placed in contact with the fiber and remains there as a result of wetting by the liquid component of the rod. When a deionized water stream locally lowers the surfactant concentration and increases the interfacial tension, the rod collapses and is pulled into wrapping around the fiber by the rod-fiber meniscus.

contrast shows the helical nature of the droplet's contact with the fiber, resulting in increased resistance to subsequent removal in flow because of the small droplet profile extending beyond the fiber surface and the large droplet contact area. Shape change by an endoskeleton droplet is irreversible when its deformation is the result of internal structural collapse.

Dilution-triggered shape change in an endoskeleton droplet is possible because of the droplet's hybrid nature, providing a liquid surface that readily wets other materials and a solid skeleton that fails only above a yield stress threshold. Fig. 8a shows the dilution-induced collapse of an endoskeleton rod onto a spherical, hydrophobic, hydrogenated castor oil particle and the advancing liquid film that pulls the collapsing drop toward the particle. Fig. 8b shows the initial glancing contact of an endoskeleton rod with a human hair that, upon dilution of the surrounding aqueous surfactant, becomes complete contact

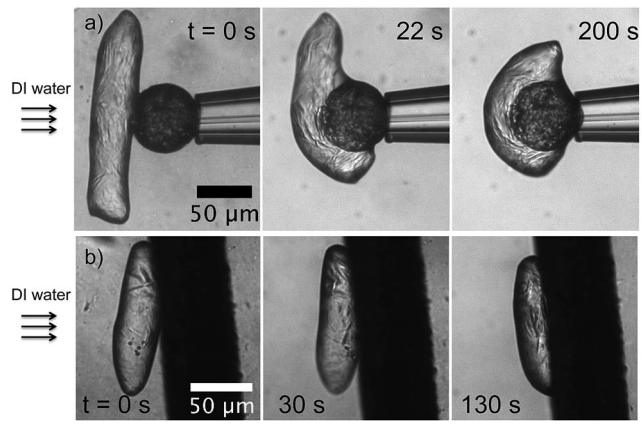

Fig. 8 (a) Top view of a collapsing endoskeleton rod wrapping around a spherical particle of hydrogenated castor oil as a result of rinsing away of local surfactant. (b) A rod in partial contact with a human hair shaft and then pulled into closer contact and wetting by rinsing with deionized water.

along the entire length of the droplet, again with a lower profile than typically presented by a spherical droplet of the same fluid. Here the raised interfacial tension triggers increased wetting and a pull toward the fiber surface, producing increased contact and adhesion without the need for structural collapse of the droplet.

4 Conclusions

Individual structured droplets, with stable rod shapes that can change in response to dilution, have been created with different size, mechanical strength, and resultant stability. The choice of liquid and internal solids requires total wetting of the latter by the former. A simple physical model of the stability, and triggered collapse, of such structures is presented and used to predict and control large-strain droplet shape-change. The model is used to develop a design basis for producing droplets that remain stable in all conditions, or that fail in response to a specific stimulus that raises the interfacial tension, like dilution. Biasing droplet collapse by first contacting it with a surface, as occurs in the use of a sprayed or spread formulation, then diluting or otherwise increasing the interfacial pressure, can trigger the collapse of the droplet onto features of the contacted surface to promote a significantly increased coverage and a decreased likelihood of removal in subsequent flow. The approach to molding anisotropic shapes in structured droplets is quite general and control over the shape change requires only awareness of the droplet rheology and the emulsion interfacial tension. Assemblies of rods that access new shapes and modes of shape-change also have the potential to provide unique benefits over solid particles, but will require new processes for multiple rod creation and assembly. Other possible applications include expanding on solid-phase results achieved by composite hydrogels[30] to direct shape-change, or lock and key colloids[31] for more targeted delivery. A structured drop matrix also potentially offers a liquid platform to optimize shapes for a given application using evolutionary methods like those developed for granular solids.[32]

Acknowledgements

PTS and MC gratefully acknowledge discussions of these results with Amar Pawar (Momentive Performance Materials), Véronique Trappe (U. Fribourg), and Todd Squires (UCSB). EMF acknowledges financial support of the National Science Foundation (CBET-1336132).

References

1 O. Velev, A. Lenhoff and E. Kaler, *Science*, 2000, **287**, 2240.
2 R. Shah, H. Shum, A. Rowat, D. Lee, J. Agresti, A. Utada, L. Chu, J. Kim, A. Fernandez-Nieves, C. Martinez, *et al.*, *Mater. Today*, 2008, **11**, 18–27.
3 D. Dendukuri, D. Pregibon, J. Collins, T. Hatton and P. Doyle, *Nat. Mater.*, 2006, **5**, 365–369.
4 T. Merkel, K. Herlihy, J. Nunes, R. Orgel, J. Rolland and J. DeSimone, *Langmuir*, 2010, **26**, 13086.

5 S. Mitragotri and J. Lahann, *Nat. Mater.*, 2009, **8**, 15–23.
6 A. Garcia, P. Mack, S. Williams, C. Fromen, T. Shen, J. Tully, J. Pillai, P. Kuehl, M. Napier, J. DeSimone, *et al.*, *J. Drug Delivery*, 2012, **2012**, 1–10.
7 S. Glotzer and M. Solomon, *Nat. Mater.*, 2007, **6**, 557–562.
8 V. Manoharan, M. Elsesser and D. Pine, *Science*, 2003, **301**, 483.
9 E. Dufresne, H. Noh, V. Saranathan, S. Mochrie, H. Cao and R. Prum, *Soft Matter*, 2009, **5**, 1792–1795.
10 T. Nguyen, E. Jankowski and S. Glotzer, *ACS Nano*, 2011, **5**, 8892–8903.
11 Z. Zhang, N. Krishna, M. Lettinga, J. Vermant and E. Grelet, *Langmuir*, 2009, **25**, 2437–2442.
12 J. Champion, Y. Katare and S. Mitragotri, *J. Controlled Release*, 2007, **121**, 3–9.
13 J. Yoo and S. Mitragotri, *Proc. Natl. Acad. Sci. U. S. A.*, 2010, **107**, 11205–11210.
14 Z. Yang, W. T. S. Huck, S. M. Clarke, A. R. Tajbakhsh and E. M. Terentjev, *Nat. Mater.*, 2005, **4**, 486–490.
15 K. Bong, D. Pregibon and P. Doyle, *Lab Chip*, 2009, **9**, 863–866.
16 J. Kim, J. Hanna, M. Byun, C. Santangelo and R. Hayward, *Science*, 2012, **335**, 1201–1205.
17 T. Leong, P. Lester, T. Koh, K. Emma and D. Gracias, *Langmuir*, 2007, **23**, 8747–8751.
18 C. Py, P. Reverdy, L. Doppler, J. Bico, B. Roman and C. Baroud, *Phys. Rev. Lett.*, 2007, **98**, 156103.
19 M. Clauzel, E. Johnson, T. Nylander, R. Panandiker, M. Sivik and L. Piculell, *ACS Appl. Mater. Interfaces*, 2011, **3**, 2451–2462.
20 P. Decuzzi and M. Ferrari, *Biomaterials*, 2006, **27**, 5307–5314.
21 O. Lieleg, M. Claessens and A. Bausch, *Soft Matter*, 2010, **6**, 218–225.
22 E. Moeendarbary, *Nat. Mater.*, 2013, **12**, 253–261.
23 A. Pawar, M. Caggioni, R. Ergun, R. Hartel and P. Spicer, *Soft Matter*, 2011, **7**, 7710.
24 A. Pawar, M. Caggioni, R. Hartel and P. Spicer, *Faraday Discuss.*, 2012, **158**, 341–350.
25 A. Abate, L. Han, L. Jin, Z. Suo and D. Weitz, *Soft Matter*, 2012, **8**, 10032–10035.
26 M. Claessens, R. Tharmann, K. Kroy and A. Bausch, *Nat. Phys.*, 2006, **2**, 186–189.
27 P. Panizza, W. Engl, C. Hany and R. Backov, *Colloids Surf., A*, 2008, **312**, 24–31.
28 A. Wierenga, A. Philipse, H. Lekkerkerker and D. Boger, *Langmuir*, 1998, **14**, 55–65.
29 M. Solomon and P. Spicer, *Soft Matter*, 2010, **6**, 1391–1400.
30 H. Thérien-Aubin, Z. L. Wu, Z. Nie and E. Kumacheva, *J. Am. Chem. Soc.*, 2013, **135**, 4834–4839.
31 S. Sacanna, W. Irvine, P. Chaikin and D. Pine, *Nature*, 2010, **464**, 575–578.
32 M. Z. Miskin and H. M. Jaeger, *Nat. Mater.*, 2013, **12**, 1–6.